



Discovery of 9-(1-anilinoethyl)-2-morpholino-4-oxo-pyrido[1,2-a]pyrimidine-7-carboxamides as PI3K β/δ inhibitors for the treatment of PTEN-deficient tumours

Bernard Barlaam^{b,*}, Sabina Cosulich^{b,†}, Sébastien Degorce^b, Martina Fitzek^b, Fabrizio Giordanetto^{c,‡}, Stephen Green^b, Tord Inghardt^c, Laurent Hennequin^{a,§}, Urs Hancox^b, Christine Lambert-van der Brempt^a, Rémy Morgentin^{a,¶}, Sarah Pass^b, Patrick Plé^a, Twana Saleh^a, Lara Ward^b

^aAstraZeneca, Centre de Recherches, Z.I. La Pompelle, B.P. 1050, Chemin de Vrilly, 51689 Reims, Cedex 2, France

^bAstraZeneca Pharmaceuticals, Oncology iMed, Alderley Park, Macclesfield, Cheshire SK10 4TG, United Kingdom

^cAstraZeneca R&D, CVMD iMed, Pepparedsleden 1, SE-431 83 Mölndal, Sweden

ARTICLE INFO

Article history:

Received 3 June 2014

Revised 11 June 2014

Accepted 13 June 2014

Available online 21 June 2014

Keywords:

PI3K β inhibitor

Rational design

PTEN-deficient tumours

ABSTRACT

Starting from TGX-221, we designed a series of 9-(1-anilinoethyl)-2-morpholino-4-oxo-pyrido[1,2-a]pyrimidine-7-carboxamides as potent and selective PI3K β/δ inhibitors. Structure–activity relationships and structure–property relationships around the aniline and the amide substituents are discussed. We identified compounds **17** and **18**, which showed profound pharmacodynamic modulation of phosphorylated Akt in the PC3 prostate tumour xenograft, after a single oral dose. Compound **17** also gave significant inhibition of tumour growth in the PC3 prostate tumour xenograft model after chronic oral dosing.

© 2014 Elsevier Ltd. All rights reserved.

Phosphoinositide-3-kinases (PI3Ks) are a class of enzymes that catalyse the phosphorylation of phosphoinositides at the 3-hydroxyl position. PI3Ks are grouped into three classes, based on their substrate specificity and structural features.¹ Class I PI3Ks are further divided into class IA enzymes (PI3K α , PI3K β and PI3K δ) and class IB enzymes (PI3K γ). Class I PI3Ks primarily generate phosphatidylinositol-3,4,5-triphosphate (PI(3,4,5)P₃), which acts as a second messenger to trigger a diverse set of signalling cascades, whilst the tumour suppressor PTEN (phosphatase and tensin homologue) reverses this process.²

The different class I isoforms of PI3K were originally thought to be redundant in function, and as such, most of the PI3K inhibitors currently in clinical trials are pan-PI3K inhibiting all four PI3K isoforms. One concern associated with pan-PI3K inhibitors is their

tolerability profile, especially given the fact that the first having entered clinical trials are not highly selective for PI3Ks. On the other hand, isoform-selective PI3K inhibitors would have the potential to completely block the relevant target while limiting toxicities associated with broader inhibition profiles.³ Moreover, the generation of isoform selective inhibitors has started to elucidate individual distinct functions for these lipid kinases. For instance, PI3K δ has been shown to play a critical role in B-cell signalling in response to a number of cytokines and chemokines. Specific inhibition of PI3K δ has been shown to have activity in human B-cell cancers such as chronic lymphocytic leukemia (CLL) and indolent non-Hodgkin lymphoma (iNHL).⁴

Specific catalytic inhibition of PI3K β has been reported to block platelet responses to shear stress and to regulate the formation of arterial thrombi.⁵ In human cancer models, inhibition of PI3K β is thought to be important in tumours which have lost PTEN, as deletion of PI3K β , but not PI3K α was shown to markedly impair tumorigenesis driven by the loss of PTEN.⁶ These results have prompted drug discovery efforts to find selective orally active PI3K β inhibitors and, as a result, many PI3K β selective inhibitors have been disclosed recently.⁷ However, at the start of this work, only few isoform selective inhibitors had been reported, mainly from the TGX series as exemplified by TGX-221.⁸ Subsequent efforts at

* Corresponding author. Tel.: +44 1625 231853.

E-mail address: bernard.barlaam2@astrazeneca.com (B. Barlaam).

[†] Current address: Novartis Institutes for Biomedical Research, WKL125.13.17, Klybeckstrasse 141, CH-4002 Basel, Switzerland.

[‡] Current address: Taros Chemicals GmbH & Co. KG, Emil-Figge-Str. 76a, 44227 Dortmund, Germany.

[§] Current address: Galderma R&D, les Templiers, 2400 route des Colles, 06410 Sophia-Antipolis, France.

[¶] Current address: Edelris, 115 Avenue Lacassagne, 69003 Lyon, France.

AstraZeneca resulted in the discovery of AZD6482,⁹ a PI3K β inhibitor showing inhibition of platelet aggregation suitable for short intravenous infusion in humans (see Fig. 1).

In addition to previously reported approaches at AstraZeneca to find orally active PI3K β inhibitors,¹¹ one option we considered was further optimisation of TGX-221 and AZD6482. From the start, we decided to remove the carboxylic acid present in AZD6482, as we considered it as the probable cause of poor exposure following oral administration (see preceding paper¹⁵). On the other hand, TGX-221 is a potent PI3K β inhibitor with similar cellular potency as AZD6482 (IC₅₀ 0.022 μ M for TGX-221 vs IC₅₀ 0.040 μ M for AZD6482) and is highly lipophilic (measured LogD_{7.4} 3.6), and, as a consequence, has poor physical and metabolic properties. Internal data showed that biological activity in this series resides essentially in one enantiomer: for AZD6482, the (*R*)-enantiomer is over 200 times more active than the (*S*)-enantiomer⁹ and the (*R*)-enantiomer of TGX-221 is more potent than the (*S*) one, as recently published by another group.^{7e} In addition, our internal work provided evidence that substitution of the aniline with small substituents could modulate PI3K β cellular potency (as illustrated in Table 1). An homology model of the PI3K β enzyme, based on available public and un-published in-house crystal structures of PI3K γ , docked with TGX-221 (*R*)-enantiomer (see Fig. 2) helped rationalise the observed SAR.¹² This homology model recapitulated key interactions typical of PI3Ks, as seen in the crystal structure of AZD6482 bound in PI3K γ (see preceding paper¹⁵) and other homology models of PI3K β reported by other groups.^{7,11} As anticipated, the oxygen of the morpholine makes a key H-bond interaction with Val854 in the hinge region and the pyridopyrimidone occupies the central part of the ATP binding site. TGX-221 adopts a T-shape conformation and induces a conformational change in the P-loop with the movement of a conserved methionine Met779, creating a small hydrophobic pocket limited by Met779 and Trp787 where the aniline of TGX-221 lies. This conformational change was first described by Knight¹³ to explain degrees of selectivity of some inhibitors among the PI3K class I family. A similar explanation was also published for ‘propeller shape’ selective PI3K δ inhibitors.¹⁴ This hypothesis is currently the most widely accepted explanation for gain of selectivity for PI3K β and PI3K δ inhibitors versus PI3K α and PI3K γ .

Previously,¹⁵ we showed that amides at the 7-position of the pyridopyrimidone core were tolerated and we disclosed initial SAR of the 9-(1-anilinoethyl)-2-morpholino-4-oxo-pyrido[1,2-*a*]pyrimidine-7-carboxamides series. The 7-position of the pyridopyrimidone points towards a hydrophilic region containing several aspartic acids in the PI3K β isoform (i.e., Asp923 and Asp937), with access to the solvent. In this letter, we describe further optimisation of this series as orally active PI3K β / δ selective inhibitors and their potential application as anticancer agents in PTEN-deficient tumour models. Selectivity among the PI3K isoforms was routinely measured with enzyme assays and the α / β selectivity was also monitored in cell assays (inhibition of Akt phosphorylation at

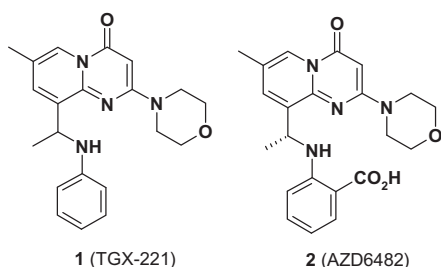
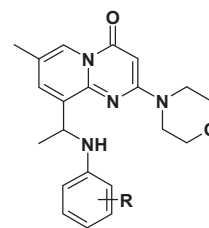


Figure 1. Structures of TGX-221 and AZD6482.

Table 1
Structure, PI3K β cellular activity of **1**, **2**, **2a–d**



Compd	R	PI3K β cell IC ₅₀ (μ M) ^a	Enantiomeric status
1 (AZD6482)	2-CO ₂ H	0.040	(<i>R</i>)
2 (TGX-221)	H	0.022	Racemic
2a	3-Me	0.081 ^b	Racemic
2b	4-F	0.19	Racemic
2c	3-Cl	0.017	Note ^c
2d	3-F, 5-F	0.009	Note ^c

^a Numbers are a geometric mean of 2 or more values.

^b *n* = 1.

^c Single enantiomer, unknown absolute configuration.

Thr308 in PI3KCA mutant human breast ductal carcinoma BT474 cells sensitive to PI3K α inhibition and at Ser473 in PTEN-null breast adenocarcinoma MDA-MB-468 cells sensitive to PI3K β inhibition).¹⁰

Compounds **3–24** were evaluated as racemates or pure enantiomers as indicated in Tables 2 and 3¹⁶ and selectivity among PI3K kinases is reported for selected compounds in Table 4. When isolated as single enantiomers, compounds **3–21** were obtained after separation of the two enantiomers by chiral preparative HPLC at the final step (see supplementary material for the conditions and characterisation used). Compounds **3–17** were synthesised according to Scheme 1. As described in the preceding paper,¹⁵ the key ester **27**, a common intermediate for all the different routes is readily available in a few steps from aminopyridine **25**. The first route relied on methyl ketone **29**, again described previously.¹⁵ From **29**, reductive amination with aniline followed by amide coupling gave **4**.¹⁷ However, for less nucleophilic anilines, the reductive amination step was too sluggish. So compounds **5–13** were made from **29** as follows: selective reduction of the methyl ketone with Luche reagent, followed by amide coupling with *N,N*-dimethylethylenediamine gave alcohol **30**. Bromination and aniline displacement, either one pot or in two separate steps, gave compounds **5–13**. However, the Heck reaction to make **29** was found troublesome in some instances. An alternative route was devised to circumvent this potentially problematic step. Again, starting from the key ester **27**, Stille coupling with tributyl (1-ethoxyvinyl)stannane gave methyl ketone **31** after hydrolysis. Formation of the imine with 4-fluoroaniline and its reduction, followed by saponification of the ester and amide coupling afforded **14**. Because of the reduced reactivity of 4-fluoroaniline, imine formation required activation with titanium tetrachloride. Therefore, an alternative route via the alcohol **32** was also used for **3**, **15–17**. Compound **31** was subjected to reduction with Luche reagent to give alcohol **32**. Bromination and displacement with the corresponding aniline, followed by saponification of the ester and amide coupling gave **3**,¹⁷ **15–17**.

Compounds **18–21** were made according to Scheme 2: from **29**, selective reduction of the methyl ketone with Luche reagent, followed by amide coupling with dimethylamine gave alcohol **33**. Bromination followed by displacement with the corresponding aniline gave compounds **18–21**. Finally, compounds **18** and **22–24** were made from carboxylic acid **34**, which derived from **32**

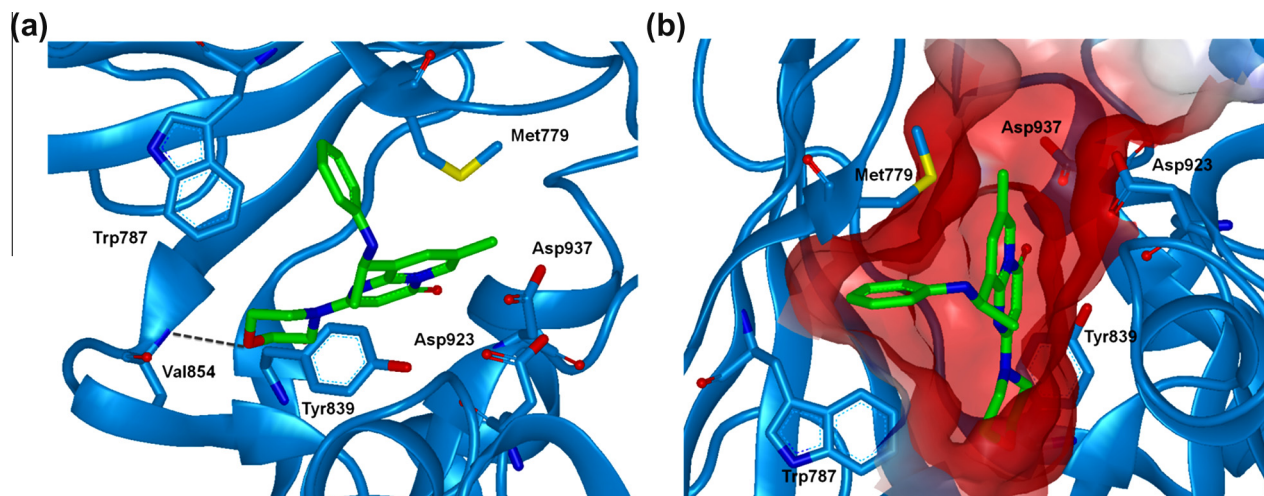
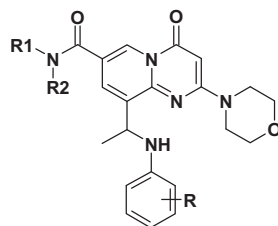


Figure 2. TGX-221, (*R*)-enantiomer docked into an homology model of PI3K β (a) Ribbon diagram showing key residues and interactions (b) Surface (in red) showing the hydrophobic pocket occupied by the aniline moiety and the solvent accessible hydrophilic channel off the 7-position of pyridopyrimidone.

Table 2
Structure, PI3K β cellular activity, permeability and lipophilicity of compounds 3–14



Compd	NR1R2	R	PI3K β cell IC ₅₀ (μ M) ^a	Caco-2 P _{app} ^b	Log D _{7.4} ^c	Enantiomeric status ^d
3	NMe ₂	—	0.156		2.4	(–)
4	NHCH ₂ CH ₂ NMe ₂	—	0.008	0.2	1.7	(–)
5	NHCH ₂ CH ₂ NMe ₂	4-Cl	0.075			Racemic
6	NHCH ₂ CH ₂ NMe ₂	3-Cl	0.010			Racemic
7	NHCH ₂ CH ₂ NMe ₂	2-Cl	0.007			Racemic
8	NHCH ₂ CH ₂ NMe ₂	4-F	0.012	0.2	1.8	Racemic
9	NHCH ₂ CH ₂ NMe ₂	3-F	0.002	0.3	2	Racemic
10	NHCH ₂ CH ₂ NMe ₂	2-F	0.023	0.8	1.9	Racemic
11	NHCH ₂ CH ₂ NMe ₂	3-CF ₃	0.074			Racemic
12	NHCH ₂ CH ₂ NMe ₂	4-Me	0.530			Racemic
13	NHCH ₂ CH ₂ NMe ₂	2-F, 3-Cl	0.004	0.9	2.7	(–)

^a Numbers are a geometric mean of 2 or more values.

^b Apparent permeability from A (pH 6.5) to B (pH 7.4) in Caco-2 cell line, 10^{–6} cm/s.

^c Log D_{7.4} obtained by shake-flask methodology.¹⁸

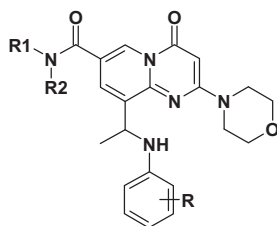
^d Optical rotation sign for compounds isolated as a pure enantiomer.

using the route described in Scheme 3. Chiral separation of the enantiomers was performed at the carboxylic acid **34**¹⁶ stage for compounds isolated as a single enantiomer (e.g., **23–24**).

An enantioselective route to **18** was also investigated (see Scheme 4): it was based on the enantioselective reduction of an imine to give enantiopure amine **37**, followed by coupling with 1-bromo-3,5-difluorobenzene via a Buchwald reaction. Several chiral auxiliaries were tried including *tert*-butylsulfonamide and phenylglycinol. The best results were obtained with (*R*)-phenylglycinol *tert*-butyldimethyl silyl ether: reaction of **29** with (*R*)-phenylglycinol *tert*-butyldimethyl silyl ether in the presence of titanium tetrakispropoxide afforded imine **35** as a mixture of *Z* and *E* isomers. Reduction of this mixture of imines with sodium cyanoborohydride at –30 °C in THF gave a 4:1 mixture of diastereoisomers. Deprotection of the silyl protecting group with TBAF

allowed easy separation of the two diastereoisomers by chromatography on silica gel. Oxidative cleavage of the major one with lead tetraacetate gave the enantiopure amine **37**. The exact configuration of **37** has not been rigorously proven at this stage. But coupling of **37** with 1-bromo-3,5-difluorobenzene under Buchwald conditions gave **18** (without evidence of racemisation). The best coupling conditions found used conditions with a catalyst¹⁹ made from xant-Phos, Pd₂dba₃ and 1-Br-3,5-F-Ph, which allowed completion of the reaction.

As previously reported,¹⁵ an amide substituent at the C-7 position of the pyridopyrimidone was tolerated as illustrated by **3** and **4**: the dimethyl amide **3** showed strong inhibition of PI3K β (IC₅₀ 11 nM) in the enzyme assay, with excellent degree of selectivity versus PI3K α (50 fold) and PI3K γ (550 fold) while keeping some PI3K δ activity (IC₅₀ 110 nM). At the cellular level, **3** retained

Table 3Structure, PI3K β cellular activity, human hepatocyte Cl_{int} , lipophilicity, solubility and permeability of compounds **14**–**24**

Compd	NR1R2	R	PI3K β cell IC ₅₀ (μ M) ^a	Human hep. Cl_{int} ^b	LogD _{7.4} ^c	Solub. μ M ^d	Caco-2 P_{app} ^e	Enantiomeric status ^f
14	NMe ₂	4-F	0.062	3	2.3	130	34	(–)
15	NMe ₂	3-F	0.039	45	ND	23	39	Racemic
16	NMe ₂	2-F, 3-F	0.073	9	2.7	28	–	Racemic
17	NMe ₂	3-F, 4-F	0.034	9	2.7	20	44	(–)
18	NMe ₂	3-F, 5-F	0.003	11	3	15	50	(R)
19	NMe ₂	3-Cl, 5-F	0.011	19	3.5	–	–	(–)
20	NMe ₂	3-F, 4-F, 5-F	0.011	13	–	10	–	(–)
21	NMe ₂	2-F, 3-F, 5-F	0.025	15	2.9	46	–	(–)
22	N(Me)CH ₂ CH ₂ OH	3-F, 5-F	0.008	10	2.1	930	–	Racemic
23	4-Morpholine	3-F, 5-F	0.025	6	2.7	316	–	(R)
24	4-Me-1-piperazine	3-F, 5-F	0.029	6	2.6	>1500	9	(R)

^a Numbers are a geometric mean of 2 or more values.^b Human hepatocyte intrinsic clearance, μ L/min/10⁶ cells.^c LogD_{7.4} obtained by shake-flask methodology.¹⁸^d Solubility from solid material, phosphate buffer (pH 7.4).^e Apparent permeability from A (pH 6.5) to B (pH 7.4) in Caco-2 cell line, 10^{–6} cm/s.^f For compounds isolated as a pure enantiomer, absolute configuration if known, otherwise optical rotation sign.**Table 4**Biological activity of compounds **3**, **4**, **13**, **14**, **17** and **18** in different PI3K enzyme and cell assays

Compd	PI3K α enz IC ₅₀ ^a	PI3K β enz IC ₅₀ ^a	PI3K γ enz IC ₅₀ ^a	PI3K δ enz IC ₅₀ ^a	PI3K α cell IC ₅₀ ^a	PI3K β cell IC ₅₀ ^a
3	0.56	0.011	6.0	0.11	9.6	0.156
4	0.37	0.008	6.9	0.085	2.2 ^b	0.008
13	0.092	0.007	0.67	0.051	0.97	0.004
14	1.3	0.037	13.5	0.23	11.6	0.062
17	0.34	0.007	3.0	0.045	4.7	0.034
18	0.075	0.005	0.51	0.032	1.2	0.003

^a μ M, numbers are a geometric mean of 3 or more values for enzyme assays and 2 or more values for cell assays.^b $n = 1$.

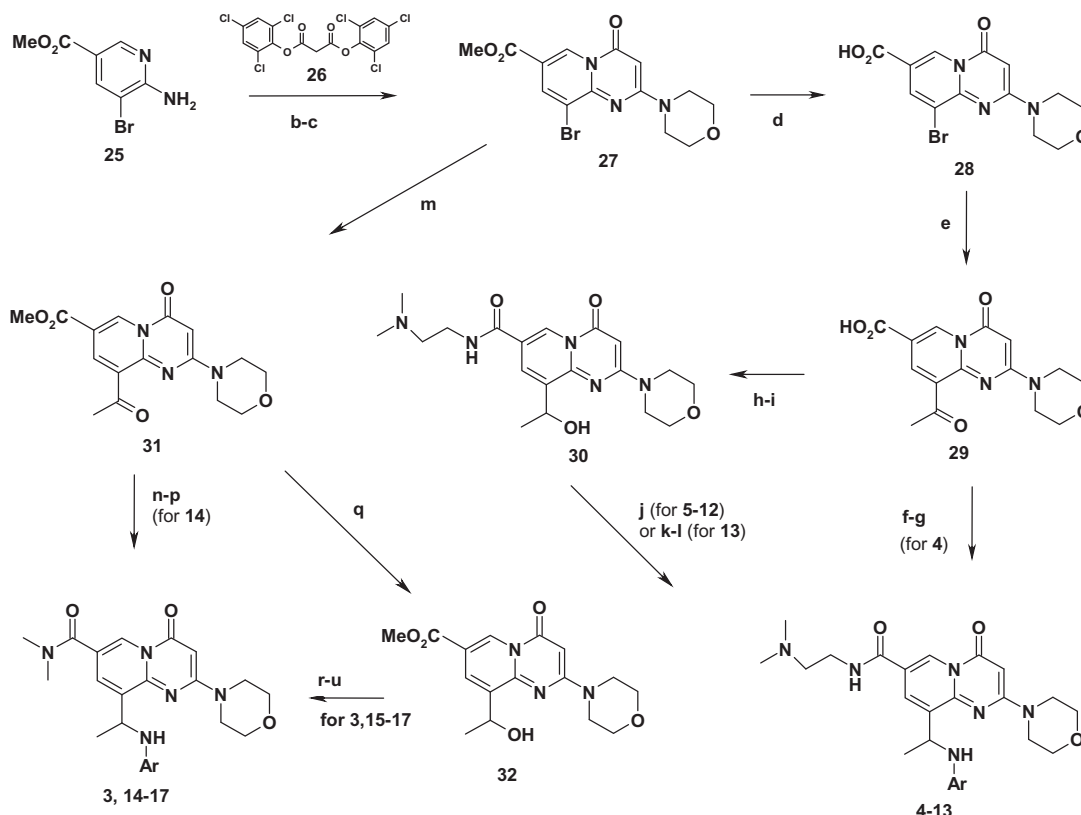
activity on PI3K β (IC₅₀ 156 nM) and good selectivity over PI3K α (60 fold), albeit potency was slightly reduced (7 fold) compared to TGX-221. The introduction of the dimethylamide group significantly reduced lipophilicity (Δ LogD_{7.4} = –1.2), making **3** a very interesting starting point. At the cellular level, the dimethylaminoethyl amide **4** was significantly more potent against PI3K β and more selective over PI3K α than the dimethyl amide **3** (IC₅₀ 8 nM, with a selectivity ratio of 270). One hypothesis for the improvement of activity and selectivity is a potential ionic interaction of the basic dimethylamino group with one of the aspartic acid in the region, most likely Asp923 in the PI3K β isoform modified as Ser919 in the PI3K α isoform. However, **4** had modest permeability in Caco-2 (P_{app} 0.2·10^{–6} cm/s).

First, we explored the structure–activity relationships of the aniline: whereas *ortho* or *meta* substitution with a chlorine was tolerated, *para*-substitution with a chlorine was poorly tolerated (see **5**, **6** and **7** vs **4**). Overall, *para*-substitution on the aniline was poorly tolerated, a fluorine being the only group maintaining similar potency: see fluoro **8** versus chloro **5** or methyl **12**. *meta* Substitution was more rewarding, a fluorine improving even cellular activity further (fluoro **9** IC₅₀ 2 nM). It is worth noting that

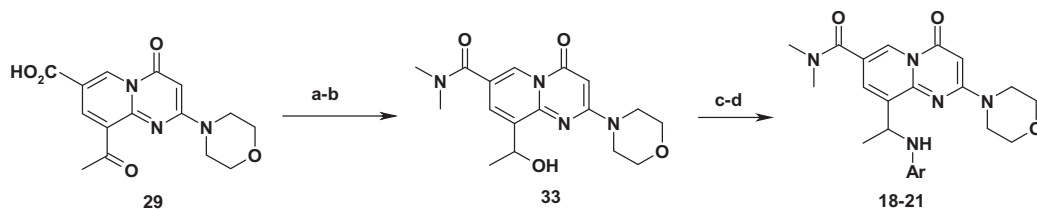
potency was reduced with larger groups (chloro **6** IC₅₀ 10 nM, trifluoromethyl **11** 74 nM). *ortho* Substitution with a fluorine also drew our attention: although **10** had slightly reduced cellular activity (IC₅₀ 23 nM), its permeability was significantly increased compared to its regioisomers (Caco-2 P_{app} 0.8·10^{–6} cm/s for **10** vs 0.2·10^{–6} cm/s for the corresponding *para*-fluoro **8** and 0.3·10^{–6} cm/s for the *meta* fluoro **9**), despite no significant change of lipophilicity. A possible explanation for the improvement of permeability is the shielding of the aniline NH by the fluorine in the *ortho* position, lowering the polar surface area. The 2-fluoro 3-chloro compound **13** combined the properties we were looking for: good potency at the cellular level (IC₅₀ 4 nM) with an exquisite selectivity versus PI3K α (240 fold at the cellular level) and improved permeability (Caco-2 P_{app} 0.9·10^{–6} cm/s). Compound **13** displayed good pharmacokinetics properties in mouse, low clearance and good bioavailability, and moderate plasma protein binding (see Table 5). At this stage, from limited modifications of the aniline from **3**, we had also identified a few neutral compounds of interest, **14** (dimethylamide, *para*-fluoro aniline) being the most prominent example: despite being significantly less potent at the cellular level (IC₅₀ 62 nM), **14** showed excellent selectivity versus PI3K α (190 fold at the cellular level), improved permeability (Caco-2 P_{app} 34·10^{–6} cm/s), low plasma protein binding and acceptable pharmacokinetics properties in mouse with good bioavailability despite a short half life ($t_{1/2}$ = 1.1 h).

Compounds **13** and **14** were evaluated in an acute pharmacodynamic experiment following a single oral dose (50 mg/kg for **13** and 100 mg/kg for **14**) in SCID mice bearing PTEN-null PC3 prostate tumour xenografts. Target modulation was assessed by measuring Akt phosphorylation levels at Ser473 at 30 min and 4 h. We saw only modest inhibition of p-Akt with **13**, despite the massive free exposure.²⁰ On the other hand, **14** delivered profound inhibition of p-Akt at both time points (see Table 6).

These results prompted us to concentrate our efforts on the neutral series derived from **3** and the substitution on the aniline was further investigated. As previously shown for the basic



Scheme 1. Synthesis of compounds **3–17**. Reagents and conditions: (a) malonic acid, 2,4,6-trichlorophenol (2 equiv), POCl₃ (2.5 equiv), 20 °C to 110 °C, 2 h (caution: gas evolution), to make **26** (crude); (b) **26** (1.2 equiv), toluene, 90 °C, 18 h, 93%; (c) MsCl (1.1 equiv), NEt₃ (1.2 equiv), THF, 10–20 °C then morpholine (3 equiv), THF, 50 °C, 82%; (d) NaOH (1.5 equiv), water, 70 °C, 1 h, 92%; (e) 4-(vinylxy)butan-1-ol (5 equiv), 1,3-bis(diphenylphosphino)propane (0.1 equiv), Pd(OAc)₂ (0.025 equiv), K₂CO₃ (2.5 equiv), DMF–water (9:1), 80 °C then **28**, 135 °C, 3 h; HCl (aq) quantitative; (f) PhNH₂ (5 equiv), AcOH, polystyrene supported trimethylammonium cyanoborohydride, DMF–water (3:1), rt, 18 h, 48%; (g) NH₂CH₂CH₂NMe₂ (2 equiv), NEt^tPr₂ (5 equiv), HATU (1.5 equiv), CH₂Cl₂, rt, 95%; chiral preparative HPLC (for **4**); (h) CeCl₃·7H₂O (1.05 equiv), MeOH–CH₂Cl₂ (2:1), then NaBH₄ (1.3 equiv), 15 °C, 15 min, 84%; (i) NH₂CH₂CH₂NMe₂ (1.05 equiv), NEt^tPr₂ (1.1 equiv), TSTU (1.2 equiv), CH₂Cl₂, rt, 1 h, 61%; (j) PBr₃ (1 equiv), ArNH₂ (6 equiv), CH₂Cl₂ or NMP, no base or K₂CO₃ (for **5–12**); (k) PBr₃ (1 equiv), CH₂Cl₂, quantitative; (l) ArNH₂ (4 equiv), NMP, 40 °C, 2 days, 66%; chiral preparative HPLC (for **13**); (m) tributyl(1-ethoxyvinyl)stannane (1.1 equiv), (PPh₃)₂PdCl₂ (0.04 equiv), dioxane, 100 °C, 18 h; 3 M HCl, 10 min; quantitative; (n) TiCl₄ (0.6 equiv), PhNH₂ (1.5 equiv), NEt₃ (3 equiv), CH₂Cl₂, 0 °C to rt, 16 h; AcOH, NaBH₃CN (1.7 equiv), CH₂Cl₂–MeOH (8:1), rt, 2 h, 61%; (o) NaOH, THF–MeOH–water, rt, 87%; (p) Me₂NH, TSTU, NEt^tPr₂, CH₂Cl₂, rt, 83% (for **14**); (q) CeCl₃·7H₂O (1 equiv), MeOH–CH₂Cl₂ (4:1), then NaBH₄ (1 equiv), rt, 5 min, 64%; (r) CH₂Cl₂, PBr₃ (1 equiv), 0 °C, 3 days, 93%; (s) ArNH₂, MeOH–CH₂Cl₂, 25–50 °C; (t) NaOH, THF–MeOH–water, rt; (u) Me₂NH, TSTU, NEt^tPr₂, CH₂Cl₂, rt (for **3** and **15–17**); chiral preparative HPLC for **3** and **17**.

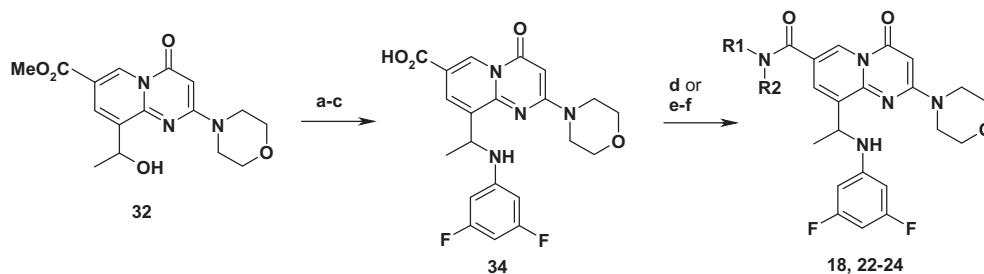


Scheme 2. Synthesis of compounds **18–21**. Reagents and conditions: (a) CeCl₃·7H₂O (1.05 equiv), MeOH–CH₂Cl₂ (2:1), then NaBH₄ (1.3 equiv), 15 °C, 15 min, 84%; (b) Me₂NH, TSTU, NEt^tPr₂, CH₂Cl₂, rt, 10 h, 71%; (c) PBr₃ (1 equiv), CH₂Cl₂, rt, 18 h, 59%; (d) ArNH₂ (1.5 equiv), PhNEt₂ (3 equiv), DMF, 50 °C; chiral preparative HPLC.

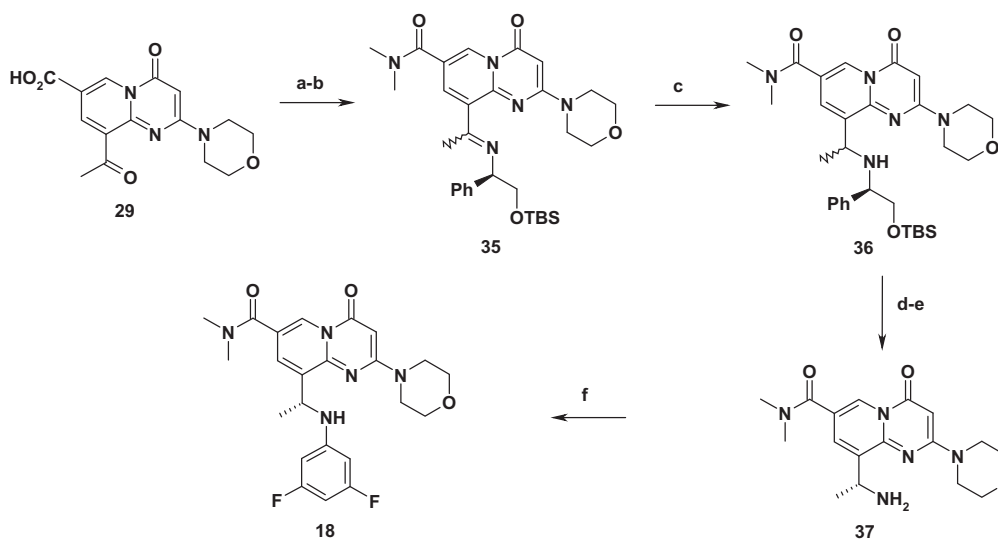
sub-series, a fluorine in the 3-position (compound **15**) gave a slight increase in cell potency, but also lowered metabolic stability. Next, we looked at bis-substitution of the aniline: both the 2,3- and 3,4-difluoro (resp. **16** and **17**) showed a similar pattern: similar cell potency as for **15**, with improved metabolic stability. However, the 3,5-difluoro **18** was 10-fold more active in cell (IC₅₀ 3 nM), with low/medium metabolic stability. Unfortunately this compound had low solubility, probably as a consequence of increased lipophilicity. Further modifications of the 3,5-difluoro-substitution of **18** were evaluated (compounds **19–21**), but all suffered from a combined reduction of both potency and metabolic stability. Modifications of the dimethylamide portion were evaluated, with the aim of improving solubility and reducing metabolic

stability further: the hydroxyethyl methyl amide **22** showed the expected solubility improvement (probably linked to the reduction of lipophilicity) and medium/low metabolic stability; other amides such morpholine **23** and *N*-methylpiperazine **24** had better metabolic stability but reduced cellular potency.

Representative compounds of the series and their activity on the different PI3K isoforms is reported in Table 4: at the enzyme level, all compounds showed potent activity against PI3Kβ and PI3Kδ isoforms, with excellent selectivity against PI3Kα and PI3Kγ. The PI3Kβ selectivity over PI3Kα was confirmed at the cellular level. We next turned our attention to the *in vivo* pharmacokinetic properties of these molecules: representative compounds were evaluated in mouse pharmacokinetics: **17** and **18** had acceptable



Scheme 3. Synthesis of compounds **18**, **22–24**. Reagents and conditions: (a) PBr_3 (1 equiv), CH_2Cl_2 , 0°C , 3 days, 93%; (b) 3,5-F- PhNH_2 (4 equiv), $\text{MeOH}-\text{CH}_2\text{Cl}_2$, 50°C , 2 days, 83%; (c) NaOH , $\text{THF}-\text{MeOH}-\text{water}$, rt, 100%; (d) $\text{HN}(\text{Me})\text{CH}_2\text{CH}_2\text{O}-\text{TBDPS}$, TSTU , NEt^iPr_2 , CH_2Cl_2 , rt; TBAF, THF , rt, 42% over 2 steps (for **22**); (e) Chiral preparative HPLC (at the carboxylic acid stage); (f) *n*-Pr-phosphonic anhydride trimer or TSTU , $\text{R}_1\text{R}_2\text{NH}$, NEt^iPr_2 , CH_2Cl_2 , rt.



Scheme 4. Enantioselective synthesis of **18**. Reagents and conditions: (a) $\text{Me}_2\text{NH}\cdot\text{HCl}$, TBUT , NEt^iPr_2 , CH_2Cl_2 , rt, 65%; (b) (*R*)- $\text{PhCH}(\text{NH}_2)\text{CH}_2\text{O}-\text{TBDMS}$, $\text{Ti}(\text{O}^i\text{Pr})_4$, THF , 70°C , 12 h (c) NaBH_3CN (0.9 equiv), AcOH (3 equiv), THF , -30°C , 2 h, diastereoisomeric mixture (*syn/anti*: 4:1); (d) TBAF (2 equiv), THF , rt; purification on silica gel (0–20% $^i\text{PrOH}$ in CH_2Cl_2), 2nd eluted isomer: 42% (over 3 steps); (e) $\text{Pb}(\text{OAc})_4$, (1.3 equiv), MeOH , 0°C , 69%; (f) Pd-catalyst (1 equiv; made from: *xant-Phos* (2.2 equiv), Pd_2dba_3 (1 equiv), 1-*Br*-3,5-F-*Ph* (9 equiv), benzene; precipitation in ether, 74%), Cs_2CO_3 (3.5 equiv), 1-*Br*-3,5-F-*Ph* (4 equiv), dioxane, 90°C , 24 h, 29%.

Table 5
Pharmacokinetic parameters in mice and protein binding of compounds **13**, **14**, **17** and **18** in mouse and human plasma

Compd	CL ^a	F% ^a	Mo/Hu ppb %free ^b
13	10	39	1.6/3.3
14	45	70	12/21
17	74	35	8.7/14
18	82	31	4.7/12

^a Mouse pharmacokinetic parameters; hairy mice dosed at $5\ \mu\text{mol/kg}$ i.v. and $30\ \mu\text{mol/kg}$ p.o.; clearance ($\text{mL}/\text{min}/\text{kg}$) and bioavailability (%).

^b Protein binding in nude mouse and human plasma, expressed as fraction unbound (%).

pharmacokinetic parameters, including bioavailability (see Table 5). Compounds **17** and **18** were subsequently administered at higher doses, respectively $200\ \text{mg/kg}$ and $100\ \text{mg/kg}$ and, despite their modest solubility, delivered sustained good plasma levels up to 8 h, possibly because of prolonged absorption in the gut. They were selected for evaluation in our acute pharmacodynamic model (single oral dose in SCID mice bearing PC3 prostate tumour xenografts). As shown in Table 6, both compounds gave very strong inhibition of p-Akt (>80% inhibition) up to 4 h with significant inhibition retained at 8 h (71% and 56% resp. for **17** and **18**).

Based on its strong and sustained pharmacodynamic inhibition of p-Akt up to 8 h following a single oral administration, the

antitumour activity of **17** at the $200\ \text{mg/kg}$ b.i.d. oral chronic dose was evaluated in the PTEN-null PC3 prostate tumour xenograft model in SCID mice: **17** showed 40% inhibition of tumour growth at the end of the experiment (see Fig. 3).

In summary, based on the docking on TGX-221 in a PI3K β homology model, we have designed a series of 9-(1-anilinoethyl)-2-morpholino-4-oxo-pyrido[1,2-*a*]pyrimidine-7-carboxamides

Table 6
Pharmacokinetic exposure, free cover over PI3K β cellular IC_{50} for compounds **13**, **14**, **17** and **18** and effect on p-Akt in a SCID mice PC3 xenograft model

Compd	Time point (h)	% Inhib p-Akt	Total plasma concn (μM) ^a	Free cover ^b
13	0.5	26	21	83
13	4	40	12	48
14	0.5	85	71	140
14	4	60	8.1	16
17	0.5	81	3.9	10
17	4	81	2.3	5.9
17	8	71	0.3	2.5
18	1	92	13	204
18	4	80	6.8	106
18	8	56	2.6	41

^a Compounds **13**, **14**, **17** and **18** were administered orally as a suspension (single dose of $50\ \text{mg/kg}$ for **13**, $100\ \text{mg/kg}$ for **14** and **18**, $200\ \text{mg/kg}$ for **17**).

^b Free cover over PI3K β cellular IC_{50} .

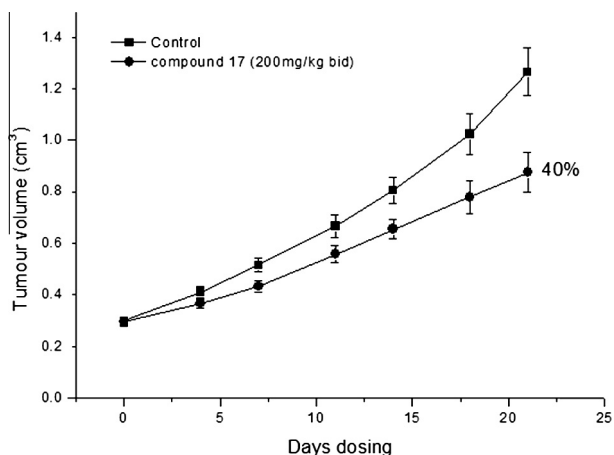


Figure 3. Tumour growth inhibition of **17** in a PTEN-null PC3 prostate tumour xenograft model in SCID mice.

as PI3K β/δ inhibitors. Optimisation of the aniline and the amide substituents led to identification of potent PI3K β/δ inhibitors with excellent selectivity versus PI3K α and PI3K γ such as **17** and **18**. Both compounds show profound pharmacodynamic modulation of p-Akt in PTEN-null PC3 prostate tumour bearing mice after oral administration and **17** gave significant inhibition of tumour growth in the same xenograft model.

Acknowledgments

We would like to acknowledge the following scientists for their contribution in the synthesis or characterization of the compounds: Christian Delvare, Delphine Dorison Duval, Myriam Didelot, Olle Karlsson, Patrice Koza, Jean-Jacques Lohmann, Mickaël Maudet, Marie-Jeanne Pasquet, Aurélien Péru, Michel Vautier, Nicolas Warin and the members of the SAR Screening Groups for generating the cell and biochemical data. We would like to thank Marie Rydén Landergrén (AstraZeneca Mölndal) for determining the absolute configuration of **18** by VCD.

Supplementary data

Supplementary data (synthetic procedure for **17** and **18**, chiral purification conditions and characterization of compounds **3–4**, **13–14**, **17–21** and **34**, and VCD protocol for determining the absolute configuration of **18**) associated with this article can be found, in the online version, at <http://dx.doi.org/10.1016/j.bmcl.2014.06.040>.

References and notes

- (a) Vanhaesebroeck, B.; Leevers, S. J.; Ahmadi, K.; Timms, J.; Katso, R.; Driscoll, P. C.; Woscholski, R.; Parker, P. J.; Waterfield, M. D. *Ann. Rev. Biochem.* **2001**, *70*, 535; (b) Vanhaesebroeck, B.; Guillermet-Guibert, J.; Graupera, M.; Bilanges, B. *Nat. Rev. Mol. Cell. Biol.* **2010**, *11*, 329.
- Georgescu, M.-M. *Genes Cancer* **2010**, *1*, 1170.
- Fruman, D. A.; Rommel, C. *Nat. Rev. Drug Discovery* **2014**, *13*, 140.
- (a) Meadows, S. A.; Vega, F.; Kashishian, A.; Johnson, D.; Diehl, V.; Miller, L. L.; Younes, A.; Lannutti, B. J. *Blood* **1897**, *2012*, 119; (b) Norman, P. *Expert Opin. Ther. Pat.* **2011**, *11*, 1773.
- Jackson, S. P.; Schoenwaelder, S. M.; Goncalves, L.; Nesbitt, W. S.; Yap, C. L.; Wright, C. E.; Kenche, V.; Anderson, K. E.; Dopheide, S. M.; Yuan, Y.; Sturgeon, S. A.; Prabakaran, H.; Thompson, P. E.; Smith, G. D.; Sheperd, P. R.; Daniele, N.; Kulkarni, S.; Abbott, B.; Saylik, D.; Jones, C.; Lu, L.; Giuliano, S.; Hughan, S. C.; Angus, J. A.; Robertson, A. D.; Salem, H. H. *Nat. Med.* **2005**, *11*, 507.
- (a) Jia, S.; Liu, Z.; Zhang, S.; Liu, P.; Zhang, L.; Lee, S. H.; Zhang, J.; Signoretti, S.; Loda, M.; Roberts, T. M.; Zhao, J. *J. Nature* **2008**, *454*, 776; (b) Wee, S.; Wiederschain, D.; Maira, S.-M.; Loo, A.; Miller, C.; DeBeaumont, R.; Stegmeier, F.; Yao, Y. M.; Lengauer, C. *Proc. Natl. Acad. Sci. U.S.A.* **2008**, *105*, 13057.

- (a) Certal, V.; Halley, F.; Virone-Oddos, A.; Thompson, F.; Filoche-Romme, B.; El-Ahmad, Y.; Carry, J.-C.; Delorme, C.; Karlsson, A.; Abecassis, P.-Y., et al. *Bioorg. Med. Chem. Lett.* **2012**, *22*, 6381; (b) Certal, V.; Halley, F.; Virone-Oddos, A.; Delorme, C.; Karlsson, A.; Rak, A.; Thompson, F.; Filoche-Romme, B.; El-Ahmad, Y.; Carry, J.-C., et al. *J. Med. Chem.* **2012**, *55*, 4788; (c) Lin, H.; Schulz, M. J.; Xie, R.; Zeng, J.; Luengo, J. I.; Squire, M. D.; Tedesco, R.; Qu, J.; Erhard, K.; Mack, J. F., et al. *ACS Med. Chem. Lett.* **2012**, *3*, 524; (d) Yu, H.; Moore, M. L.; Erhard, K.; Hardwicke, M. A.; Lin, H.; Luengo, J. I.; McSurdy-Freed, J.; Plant, R.; Qu, J.; Raha, K., et al. *ACS Med. Chem. Lett.* **2013**, *4*, 230; (e) Lin, H.; Erhard, K.; Hardwicke, M. A.; Luengo, J. I.; Mack, J. F.; McSurdy-Freed, J.; Plant, R.; Raha, K.; Rominger, C. M.; Sanchez, R. M., et al. *Bioorg. Med. Chem. Lett.* **2012**, *22*, 2230; (f) Hardwicke, M. A.; Ariazi, J.; Bushdid, P.; Erhard, K.; McSurdy-Freed, J.; Lin, H.; Luengo, J.; Mack, J.; Pietrak, B.; Plant, R.; Qu, J.; Raha, K.; Rominger, C.; Sanchez, R. M.; Schaber, M. D.; Schulz, M. J.; Sherck, C.; Sinnamon, R.; Skordos, K.; Spengler, M.; Squire, M.; Tedesco, R.; Xie, R.; Yu, H.; Zeng, J.; Rivero, R. A. *Abstract MEDI 21*, 243rd ACS National Meeting, San Diego, CA, March 25–29, 2012.
- Jackson, S. P.; Robertson, A. D.; Kenche, V.; Thompson, P.; Prabakaran, H.; Anderson, K.; Abbott, B.; Goncalves, L.; Nesbitt, W.; Schoenwaelder, S.; Saylik, D. *PCT Int. Appl.* **2004**, WO2004016607.
- Nylander, S.; Kull, B.; Björkman, J. A.; Ulvinge, J. C.; Oakes, N.; Emanuelsson, B. M.; Andersson, M.; Skåby, T.; Inghardt, T.; Fjellström, O.; Gustafsson, D. J. *Thromb. Haemost.* **2012**, *10*, 2127.
- For description of the PI3K enzyme assays (α , β , γ and δ isoforms) and the PI3K β cell assay (inhibition of Ser473 Akt phosphorylation endpoint in breast adenocarcinoma MDA-MB-468 cells), see: Barlaam, B. C.; Degorce, S. L.; Lambert-Van der Brempt, C. M. P.; Morgentin, R.; Ple, P. *U.S. Pat. Appl. Publ.* **2011**, US20110098271.
The PI3K β enzyme assay, as configured, reaches the tight binding limit for some inhibitors in Table 4. Copeland R. A., *Enzymes*, 2nd ed.; Wiley-VCH: New York, 2000; pp 305–317. In order to determine the tight binding limit for the PI3K β enzyme assay, the concentration of functional enzyme for the PI3K β isoform was determined experimentally. The tight binding limit is half the concentration of functional enzyme, which gives a tight binding limit of 10 nM for PI3K β .
PI3K α cell assay (inhibition of Tyr308 Akt phosphorylation endpoint in human breast ductal carcinoma BT474 cells): BT474 cells were seeded into black 384 well plates at a density of 5600 cells/well in DMEM containing 10% FCS and 1% glutamine and allowed to adhere overnight. The following morning compounds in 100% DMSO were added to assay plates by acoustic dispensing. After a 2 h incubation at 37 °C and 5% CO₂ the medium was aspirated and the cells were lysed with a buffer containing 25 mM Tris-HCl, 3 mM EDTA, 3 mM EGTA, 50 mM sodium fluoride, 2 mM sodium orthovanadate, 0.27 M sucrose, 10 mM β -glycerophosphate, 5 mM sodium pyrophosphate, 0.5% Triton X-100 and complete protease inhibitor cocktail tablets (1 tab per 50 mL lysis buffer). After 20 min, the cell lysates were transferred into ELISA plates which had been pre-coated with an anti total Akt antibody in PBS buffer and non-specific binding blocked with 1% BSA in PBS buffer containing 0.05% Tween 20. Plates were incubated overnight at 4 °C. The next day the plates were washed with PBS buffer containing 0.05% Tween 20 and further incubated with a mouse monoclonal anti-phospho Akt Thr308 for 2 h. Plates were washed again as above before addition of a horse anti-mouse-HRP conjugated secondary antibody. Following a 2 h incubation at room temperature, plates were washed and QuantaBlu substrate working solution was added to each well. The developed fluorescent product was stopped after 60 min by addition of Stop solution to the wells. Plates were read using a Tecan Safire plate reader using 325 nm excitation and 420 nm emission wavelengths, respectively.
- (a) Giordanetto, F.; Kull, B.; Dellsen, A. *Bioorg. Med. Chem. Lett.* **2011**, *21*, 829; (b) Giordanetto, F.; Waallberg, A.; Cassel, J.; Ghosal, S.; Kossenjans, M.; Yuan, Z.-Q.; Wang, X.; Liang, L. *Bioorg. Med. Chem. Lett.* **2012**, *22*, 6665; (c) Giordanetto, F.; Waallberg, A.; Ghosal, S.; Iliofski, T.; Cassel, J.; Yuan, Z.-Q.; von Wachenfeldt, H.; Andersen, S. M.; Inghardt, T.; Tunek, A., et al. *Bioorg. Med. Chem. Lett.* **2012**, *22*, 6671.
- The PI3K β homology model was built from a PI3K γ structure co-crystallised with 2-morpholin-4-yl-7-phenyl-4H-chromen-4-one (pdb code 1E7V; Walker, E. H.; Pacold, M. E.; Perisic, O.; Stephens, L.; Hawkins, P. T.; Wymann, M. P.; Williams, R. L. *Mol. Cell* **2000**, *6*, 909) using the PRIME homology modelling program. Prime, 1.0 ed.; Schrödinger, Inc. Compound (R)-1 ((R)-TGX-221) was docked manually by analogy to the binding mode of available public and unpublished in-house crystal of PI3K γ . Images in have been created in VIDA v4 from OpenEye Scientific Software, 3600 Cerrillos Rd., Suite 1107, Santa Fe, NM87507.
- Knight, Z. S.; Gonzalez, B.; Feldman, M. E.; Zunder, E. R.; Goldenberg, D. D.; Williams, O.; Loewith, R.; Stokoe, D.; Balla, A.; Toth, B.; Balla, T.; Weiss, W. A.; Williams, R. L.; Shokat, K. M. *A. Cell* **2006**, *125*, 733.
- Berndt, A.; Miller, S.; Williams, O.; Le, D. D.; Houseman, B. T.; Pacold, J. I.; Gorrec, F.; Hon, W.-C.; Ren, P.; Rommel, C.; Gaillard, P.; Rückle, T.; Schwartz, K. M.; Shokat, K. M.; Shaw, J. P.; Williams, R. L. *Nat. Chem. Biol.* **2010**, *6*, 117.
- Giordanetto, F.; Barlaam, B.; Berglund, S.; Edman, K.; Karlsson, O.; Lindberg, J. A.; Nylander, S.; Inghardt, T. *Bioorg. Med. Chem. Lett.* **2014**, preceding paper.
- When the enantiomers were separated, activity resided mainly in one enantiomer, with the other enantiomer being significantly less active (data not reported), as previously described for **1** and **2**. The absolute configuration of **18** was determined to be (R) by vibrational circular dichroism (VCD). Coupling of the (–) enantiomer of carboxylic acid **34** with dimethylamine gave

- 18** as a single enantiomer. This same (–) enantiomer was used to make **23** and **24**.
- Compounds **3** and **4** are the (–) enantiomers of compounds **10** and **14** from the preceding paper (Ref. 15).
 - LogD_{7.4} was measured using shake-flask methodology with a buffer/octanol volume ratio of 100:1. The concentration of compound in the aqueous phase before and after partitioning with octanol was determined by generic HPLC analysis.
 - Yin, J.; Buchwald, S. L. *J. Am. Chem. Soc.* **2002**, *124*, 6043.
 - Although tumour levels have not been assessed for **13**, we have seen high total tumour levels for related compounds carrying the same basic side chain and with similar permeability. However, we suspect that high efflux potential (MDR-mdck efflux ratio: 15) associated the moderate permeability seen with **13** may limit engagement of the target in the tumour.